Application of graphite nanoplatelet-based and nanoparticle composites to thermal interface materials

Tien-Chan Chang[1], *Yiin-Kuen Fuh*[2], *Sheng-Xun Tu*[2], *Yueh-Mu Lee*[1]

[1]*Department of Nuclear Instruments, Institute of Nuclear Energy Research, Atomic Energy Council, Executive Yuan, No. 1000, Wenhua Road, Jiaan Village, Longtan Township, Taoyuan County 32546, Taiwan*
[2]*Department of Mechanical Engineering, National Central University, No. 300, Jhongda Road, Jhongli City, Taoyuan County 32001, Taiwan*
E-mail: mikefuh@ncu.edu.tw

Published in Micro & Nano Letters; Received on 15th January 2015; Revised on 10th March 2015; Accepted on 1st April 2015

Thermal interface materials (TIMs) are of crucial importance in improving and enhancing heat transfer in electronic packages, particularly in high-density electronics at regions of exceedingly high temperatures. Commercial TIMs are generally composed of highly conductive particle fillers such as highly thermally conductive graphite and a matrix so that efficient heat transfer and good compliance of the interface material can be achieved during application. Two types of TIMs are tested based on the hybridisation of graphite nanoplatelets (GNPs) and nanoparticles (NPs). The hybrid materials are fabricated via screen printing process to ensure conformal uniformity of NPs spreading on the GNPs. The performance of fabricated materials such as temperature, applied pressure, heat flux and TIM thickness are concurrently tested in the temperature range 40–80°C and the pressure range 0–5.6 kgf/cm^2 using a standard TIM tester. The steady-state heat flow technique of American Society for Testing and Materials (ASTM) D5470–06 is fully adopted. For a thickness of 160 μm composite with three-layer GNPs and two-layer NPs, thermal conductivity is measured at ∼0.2 W/m K. In addition, the measured trend in the change of specific thermal conductivity with pressure corresponds well with the data presented in the literature.

1. Introduction: To minimise contact thermal resistance between heat-generating electronic components and a variety of cooling systems such as heat sinks and heat pipes, thermal interface material (TIM) has been widely adopted and routinely used [1–5]. In particular, a TIM is regularly used to enhance heat transfer between the direct bonded copper substrate under the semiconductor chips and/or a base-plate/heat sink [6]. As a result of inadequate thermal management of an electronic device, unacceptable temperature levels may adversely affect device performance, reliability and lifespan [7]. Therefore, accurate quantification of the thermal characteristics of new-generation TIM materials is critically important since the fundamental knowledge of the thermal, mechanical and electrical performance is essential to the proper design of electronic systems and packages [8]. In particular, heat dissipation in power electronic devices such as ultra-fast computer chips, high-power light-emitting diodes, high-power lasers and insulated gate bipolar transistors has become an urgent issue [9, 10]. TIMs are found to be beneficial as efficient interface materials between computer chips and heat sinks because of the benefits of fast heat dissipation in high-power devices [2, 11]. Moreover, in the advanced high-density electronic packaging, TIMs are crucial components to minimise overheating and thus prevent the failure of electronic components [1, 12]. Conventionally, available TIMs are manufactured by adopting highly thermally conductive fillers into the polymer matrix [13–15]. With the prominent rise of graphene [16] and graphite exfoliation technique [17, 18], members of the graphite materials family such as graphite nanoplatelets (GNPs) have also been receiving significant focus as new forms of thermally conducting filler [19–22]. GNPs are two-dimensional (2D) high aspect ratio nanoparticles (NPs) possessing advantages such as relatively high thermal conductivity such that a very efficient heat conduction pathway can be formed in polymer matrices. One example of such GNPs was recently demonstrated by the preparation of a GNP paper, the through-plane thermal conductivity of which was measured to be <1 W/m K, whereas the in-plane thermal conductivity was 100 W/m K [23, 24]. Another example of using materials of GNP–epoxy thin films with an in-plane thermal conductivity of ∼4.5 W/m K, whereas the through-plane thermal conductivity was in the range of 0.5–0.9 W/m K [25]. In this Letter, we propose a hybrid composite which consists of various layers of GNPs and NPs. Experimental measurements are systematically conducted to characterise the GNPs-based TIMs.

2. Experimental on equations: The heat conducted through the sample can be calculated by prior known thermal conductivity of meter bars and insulation to materials. The apparent specific thermal resistance or otherwise referred to as thermal impedance (RA) of the TIM can be calculated as follows

$$\mathrm{RA} = \frac{A(T_{\mathrm{S.L.}} - T_{\mathrm{S.U.}})}{Q} \tag{1}$$

where A is the cross-sectional area of the meter bars, $T_{\mathrm{S.L.}}$ and $T_{\mathrm{S.U.}}$ are the extrapolated contact surface temperatures and Q is the applied heat flux. Additionally, the effective thermal conductivity of joint (K_{eff}) can then be calculated accordingly as follows

$$K_{\mathrm{eff}} = \frac{QL}{A(T_{\mathrm{S.L.}} - T_{\mathrm{S.U.}})} = \frac{L}{R} \tag{2}$$

3. Experimental procedure: The TIM layer is designed to provide efficient heat flow from the heat-generating substrates to the heat sink in the direction normal to the thermal interface, as shown in Fig. 1*a*. Thus, in such applications, the thermal interface plane with the high through-plane thermal conductivity would be the preferred orientation. In particular, this research aims to investigate systematically the hybrid composites of both GNPs and NPs, which includes GNPs of one layer (Fig. 1*b*), two layers parallel orientations (Fig. 1*c*), three layers parallel orientations (Fig. 1*d*), GNPs two layers sandwiched NPs thermal grease (Fig. 1*e*) and GNPs three layers sandwiched two layers NPs

doi: 10.1049/mnl.2014.0689

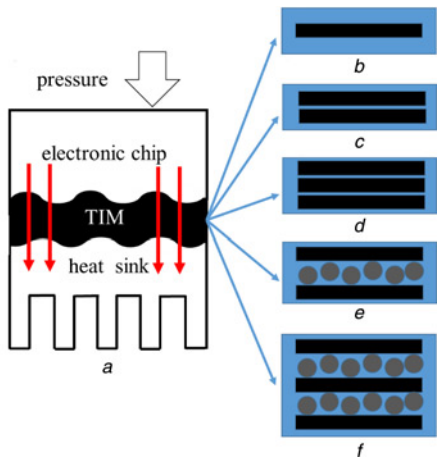

Figure 1 *Preparation of GNPs/NPs fillers used as a thin TIM in electronic packaging applications*
a Schematic showing the utilisation of TIM layer for heat removal in electronic packaging. Possible combinations of GNPs/NPs in thin TIM layer
b GNPs (one layer)
c GNPs (two layers)
d GNPs (three layers)
e GNPs two layers sandwiched NPs thermal grease
f GNPs three layers sandwiched two layers NPs thermal grease

thermal grease (Fig. 1*f*). By the principle of capillary flow for filling the porosities, the thin TIM layer can be formed by spreading the material between the contacting surfaces under pressure [1]. One notable attribute for the typical TIM material is the large difference of anisotropic thermal conductivities. For example, an in-plane thermal conductivity of 100 W/m K is compared with the through-plane thermal conductivity in the order of 1 W/m K [26]. Similar anisotropic heat conductance was also demonstrated recently in boron nitride platelet thin films [27].

Fig. 2 shows both schematic and optical photographs of the TIM apparatus for measuring thermal conductivity. The main construction includes two meter bars centred in both the upper/lower half with predefined drilled thermocouple holes, the concentrica insulation shroud (shown in black), the guard heater and the heat sink beneath the lower meter bar. To make sure of good insulation such that only heat conduction exists between the test film

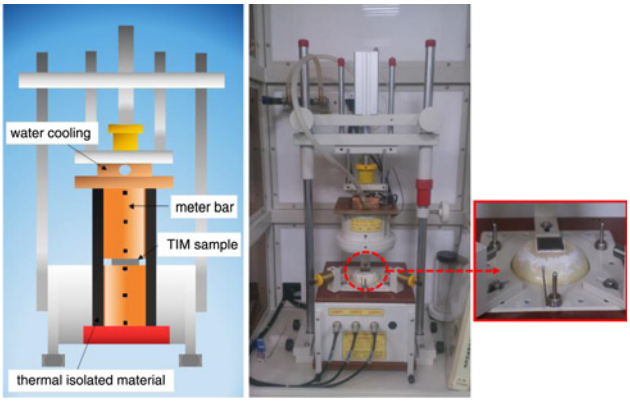

Figure 2 *TIM measuring apparatus*
a Cross-sectional schematic of the TIM apparatus for measuring thermal conductivity
Structurally, two meter bars centred in both the upper/lower half, the thermocouple holes are drilled along the centre of the meter bars, the insulation shroud (in black), the guard heater and the heat sink beneath the lower meter bar
b Optical photograph of TIM system assembly with micrometer for TIM thickness measurements in the inset in red rectangle

between the lower and upper metal bars, an overlapping joint is incorporated and fully coupled between the upper and lower insulation pieces and this overlapping joint juncture is offset from the sample location. In this manner, the heat losses between the surrounding and the assembly can be minimised and the insulation can preserve 1D heat conduction through the meter bars. Moreover, shown in the inset of Fig. 2*b* is the micrometer for measuring the *in situ* displacement when a thin TIM layer is applied at the interface. For each micrometer measurement during a typical test, thermal expansion and pneumatic compression offset were regularly calculated so that the effects of temperature and the applied pressure were properly scaled. The measurement of thermal resistance requires a 30–40 min warm-up and reaches steady state after an additional 10 min. The average of two resistance values calculated using the upper and lower heat flux measurements separately are the obtained measured resistance value. The apparatus accuracy was validated by correlating the bar surface to surface thermal conductivity measurement with theoretical predictions.

The through-plane thermal conductivity of the GNPs/NPs composites of thicknesses in the range of 35–160 µm were measured with an LW-9389 TIM Tester (Longwin, Taiwan) in the temperature range 30–80°C, which operates on the basis of the steady-state heat flow technique according to American Society for Testing and Materials (ASTM) D5470–06. The bulk through-plane thermal conductivity is calculated from the slope of the thermal resistance against thickness, which was generally observed to be linear in the thickness direction. As shown in Fig. 3, the heat flow and temperature across the TIM layer can be reliably obtained along the direction of thermal gradient utilising a set of precision thermometers. Miniature differential thermocouples were utilised to measure the temperature gradients across the GNP/NP composites.

To determine the accuracy of linear temperature gradient and the estimated heat flux, a numerical simulation was constructed using the commercial COMSOL software 4.4 (Fig. 4). In this simulation, the boundary conditions at both the top/bottom of the meter bars are extrapolated from the experimental thermocouple temperatures. The simulation is mainly to be used for estimating the conduction losses to the perimeters and validating the efficacy of 1D conduction through the meter bar. This simulation is crucial since an accurate calculation of contact resistance is highly dependent on an accurate calculation of the temperature in the apparatus. Simulation results show that for the data acquired for 2100 s, the steady state, measured temperatures fluctuation is <0.4°C. The design stage uncertainty in thermal resistance is 0.5% based on the thermocouple temperature uncertainty and variation in the recorded data. Scatter in the experiment indicates an uncertainty of 3% confidence in thermal resistance. This scatter is attributed to variation in TIM thickness, partial misalignment of heater bars and a variation in pressure at the interface. The thermal interface thickness was measured with the micrometer to 1 µm resolution. The thickness

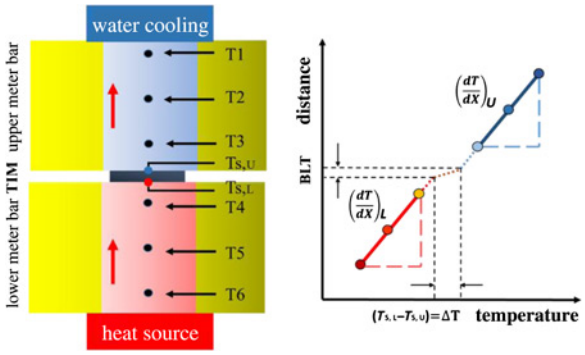

Figure 3 *TIM apparatus measures R_{TIM} using six K-type thermocouples to extract the thermal gradient along upper and lower meter bars*
Temperature drop at the interface is extrapolated from the gradient

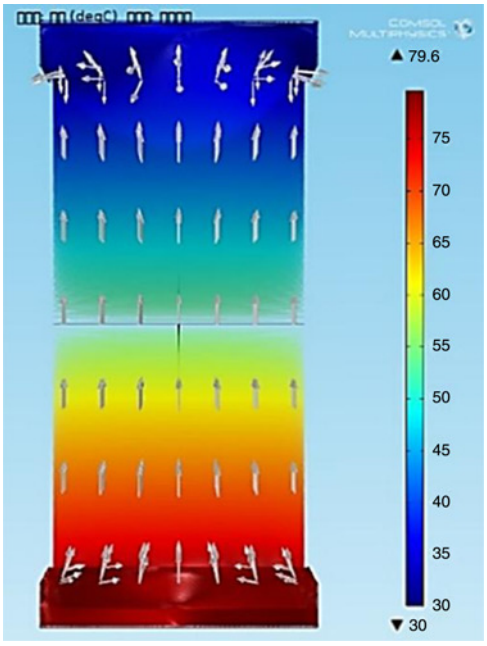

Figure 4 *COMSOL software 4.4 simulation of the temperature profile through the test section*
Test section in the centre shows 1D conduction while the insulation and guard heater protect the system from radiation and convection losses

measurement was calibrated for thermal expansion and pressure-induced compression of meter bars. The best estimate of thickness uncertainty is 1 μm [28] while the sample thicknesses vary from 35 μm. This results in some scatter in R_{TIM} calculations. Misalignment and pressure variation were tested qualitatively with pressure-sensitive paper and minimised as much as possible.

3.1. Screen printing process: The traditional TIM fabrication process adopts a subtractive process based on the photolithographic technique [29]. In comparison, the proposed screen printing allows additive-type patterning, which is widely used owing to its high machine reliability, low cost of screen mask and simple fabrication process [30]. NPs embedded GNPs composites are fabricated by a simple screen printing process with predefined mesh patterns such that the NPs can be uniformly deposited on the GNPs substrate. In this process, NPs thermal grease initially flows through a screen mesh by using a squeegee. Non-image areas on the screen are blocked, while NPs thermal grease can only print on the appropriate substrate region with the required NPs thermal grease quantity [31]. In this Letter, the NPs thermal grease thickness can be reliably controlled in 30 μm with uniformly distributed in the matrix GNPs. The microstructure analysis will be performed in the next section.

Scanning electron microscopy (SEM) study was conducted utilising JEOL-JEM2100 high-resolution SEM. To investigate the integrity of the substrate and related morphology, we conducted SEM studies of the cross-sections of the GNP films. Figs. 5*a* and *b* show the SEM image of as-received GNPs. It shows wrinkled, curled, overlapped stacks of GNPs. Furthermore, using the various magnifications, it is shown in Figs. 5*c* and *d* that the GNPs are stacks of 50–60 layers of GNPs with average thickness of 25–30 nm. This clearly indicates preferential in-plane orientation of the GNPs and the observed anisotropy of electrical and thermal conductivities can be expected if no further treatments are undertaken, such as deposit the NPs to enhance through-plane conductivity.

The SEM image in Fig. 6*a* shows the morphology of NPs of different sizes after the screen printing process. Fig. 6*b* shows the SEM microphotographs of NPs size ~300–500 nm; the scale bar is 1 μm.

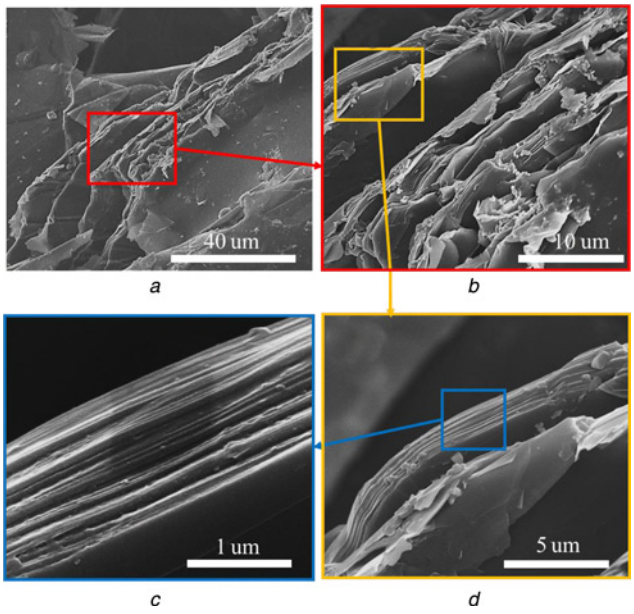

Figure 5 *SEM study of GNPs morphology in thin thermal interface layers*
SEM images of the cross-section of a thin layer of the GNPs thin film at different magnifications with scale bars
a 40 μm
b 10 μm
c 5 μm
d 1 μm

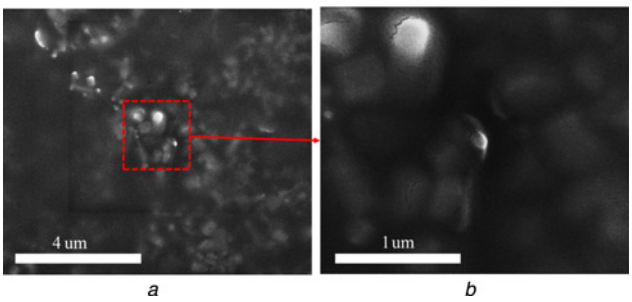

Figure 6 *SEM images of NPs at different magnifications with scale bars*
a 4 μm
b 1 μm

This further confirms that well-dispersed NPs are successfully screen printed on the GNPs and the success of our powder preparation processes.

Fig. 7*a* shows the SEM image of NPs/GNPs composite. Figs. 7*b–f* show the X-ray mapping that demonstrates that different elements (carbon, oxygen, silicon and zinc) are able to uniformly distribute in the matrix. The presence of NPs is hard to detect using energy-dispersive X-ray spectrometer (EDS) because of their low content. However, X-ray mapping was used to confirm the presence and dispersion of carbon, oxygen, silicon and zinc in the composite.

4. Results and discussion: Fig. 8 shows the changes in specific thermal resistance as a function of pressure for the fixed thermal heat flux Q (34 W) Here, one can observe a gradual decrease in thermal resistances initially as the contact pressure is increased. R_{TIM} of the hybrid composites of various layers of GNPs (one to three layers) and NPs (one and two layers) as presented in Fig. 8 clearly indicates a decreasing trend with the increase of applied pressure. The trend in the change in specific thermal resistance with pressure is inconsistent with the data presented

doi: 10.1049/mnl.2014.0689

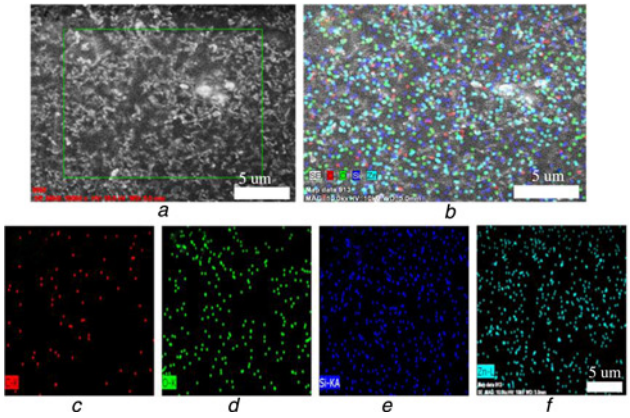

Figure 7 *SEM image and X-ray mapping analysis*
a SEM image of NPs composite
b NPs composite X-ray mapping
c Carbon X-ray mapping
d Oxygen X-ray mapping
e Silicon X-ray mapping
f Zinc (NPs) X-ray mapping

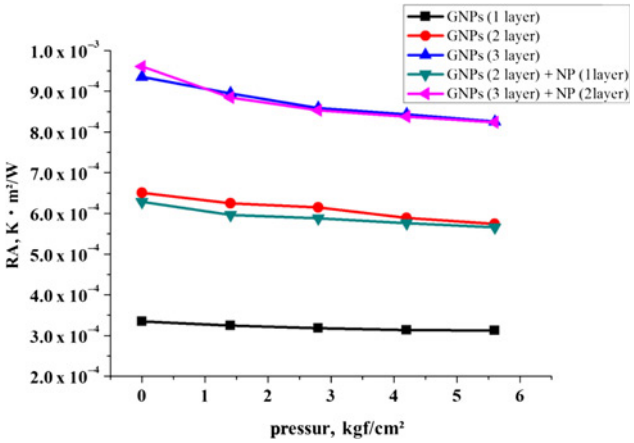

Figure 8 *Total thermal resistance per unit surface area, R_{TIM}, of hybrid composites of GNPs (one to three layers) and NPs (one and two layers) as TIM mixtures over the applied pressure range*

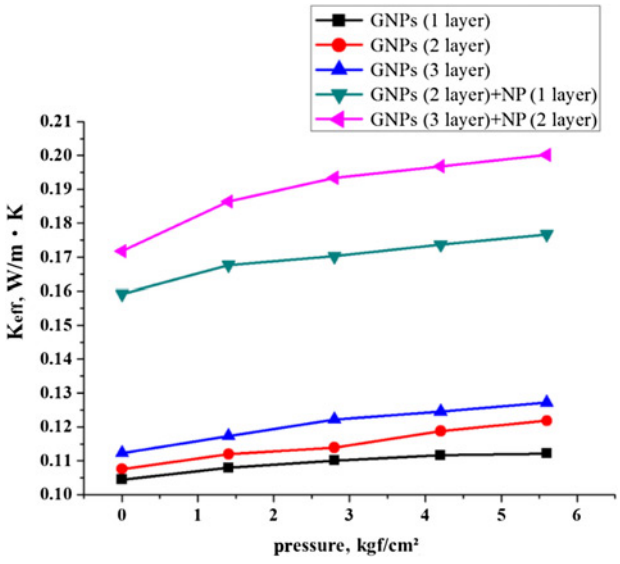

Figure 9 *Change in effective thermal conductivity with applied pressure for GNPs (one to three layers) and NPs (one and two layers)*

by Yovanovich [32]. A minimum thermal resistance of 3.12×10^{-4} K m^2/W was measured with GNPs (one layer, for a thickness of 35 μm) at an applied pressure of 5.6 kgf/cm^2. Under the same applied pressure, the thermal resistance of two layers GNPs was 5.74×10^{-4} K m^2/W for a thickness of 70 μm, three layers GNPs was 8.25×10^{-4} K m^2/W for a thickness of 105 μm, two layers GNPs + one layer NPs was 5.65×10^{-4} K m^2/W for a thickness of 100 μm and three layers GNPs + 2 layer NPs was 8.24×10^{-4} K m^2/W for a thickness of 160 μm. Generally, with the hybrid composite of GNPs (three layers) + NPs (two layers) it has been shown that the measured thermal resistance is comparatively high with all other specimens because of the increase in thickness. However, the heat transfer enhancement of proposed GNPs (three layers) + NPs (two layers) should be further investigated in the next section by applying the concept of equivalent thermal conductivity.

The change in apparent thermal conductivity of the hybrid composites of various layers of GNPs (one to three layers) and NPs (one and two layers) TIM as a function of pressure is shown in Fig. 9. The best thermal conductivity of ~0.2 W/m K at an applied pressure of 5.6 kgf/cm^2 for a thickness of 160 μm can be obtained by combining GNPs (three layers) and NPs (two layers) as the TIM. Thermal conductivity is increased with reducing thermal resistance with GNPs (three layers) + NPs (two layers) and the result is consistent with (2), under conditions of a constant thickness. Previous study using materials of GNP–epoxy thin films reported an in-plane thermal conductivity of ~4.5 W/m K, whereas the through-plane thermal conductivity was in the range of 0.5–0.9 W/m K [25]. In comparison, the proposed TIM composites produced the through-plane thermal conductivity in the range of 0.1–0.2 W/m K. The thermal conductivity is comparatively lower because the NPs have very little contents (as shown in Fig. 7 of EDS). The performance can be further improved by adopting metallic-based NPs so that the overall thermal conductivity of GNP-based TIM composite should be increased. Another aspect indicates that the thermal conductivity in materials such as graphite (2000 W/m K) and copper (~400 W/m K) can be very high; most of the previous measurements were performed for the in-plane direction [33, 34]. Therefore, the in-plane thermal conductivity will be tackled in future works for the proposed TIM materials.

A comparison between the specific thermal contact resistance for the meter bars in GNPs (one to three layers) and NPs (one and two layers) as a TIM with heat flux is shown in Fig. 10. The meter bars at a pressure of ~5.6 kgf/cm^2 are able to achieve lower thermal resistance by displacing any air in the microscopic voids of the contact zone. Here, the inclusion of GNPs is measured as the

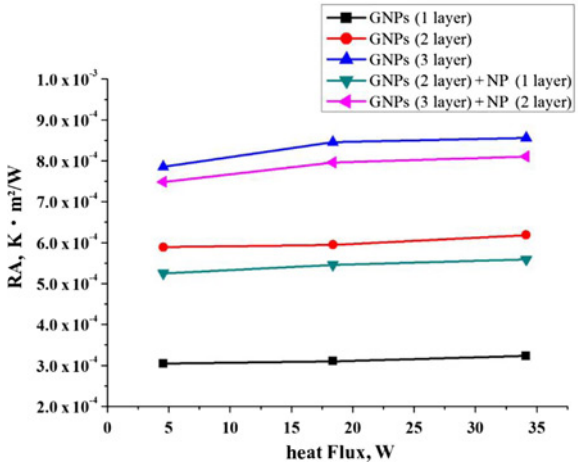

Figure 10 *Specific thermal resistance as a function of heat flux for different mixture GNPs (one to three layers) and NPs (one and two layers) as a TIM self-contact ($P \sim 5.6$ kgf/cm^2)*

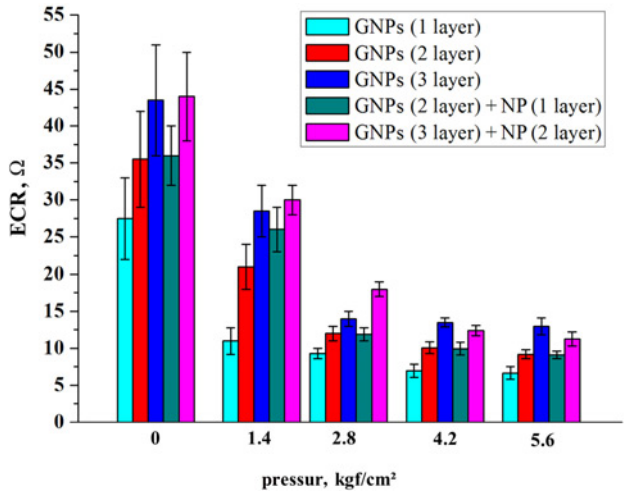

Figure 11 *Change in specific electrical contact resistance with applied pressure for GNPs (one to three layers) and NPs (one and two layers) as a TIM*

thermal contact resistance from $\sim 7.4 \times 10^{-4}$ K m^2/W with GNPs (three layers) + NPs (two layers). From the experimental trend, the slight increase in specific thermal resistance can be attributed to heat flux increase because of thickness increases in thermal expansion as the temperatures increase.

Fig. 11 presents the specific electrical contact resistance with applied pressure for GNPs (one to three layers) and NPs (one and two layers). We can observe a marked decrease in electrical resistances initially as the contact pressure is increased. The lowest electrical resistance measured was 11.25 Ω three layers GNPs + two layer NPs for a thickness of 160 µm at an applied pressure of 5.6 kgf/cm^2. Under the same thickness and sample, the electrical resistance was 12.4 Ω at an applied pressure of 4.2 kgf/cm^2, the electrical resistance was 18 Ω at an applied pressure of 2.8 kgf/cm^2, the electrical resistance was 30 Ω at an applied pressure of 1.4 kgf/cm^2 and the electrical resistance was 44 Ω at an applied pressure of 0 kgf/cm^2. The trend in the change in specific electrical resistance with pressure and the overall magnitude also correspond well with the data presented by Yovanovich [32].

GNPs (one to three layers) and NPs (one and two layers) TIM nominally 35–160 µm thick were characterised and plotted for electrical resistance against thermal resistance as a function of applied pressure and heat flux Q 34 W, as shown in Fig. 12. From the experimental result, one can observe a marked decrease in both resistances initially as the contact pressure is increased.

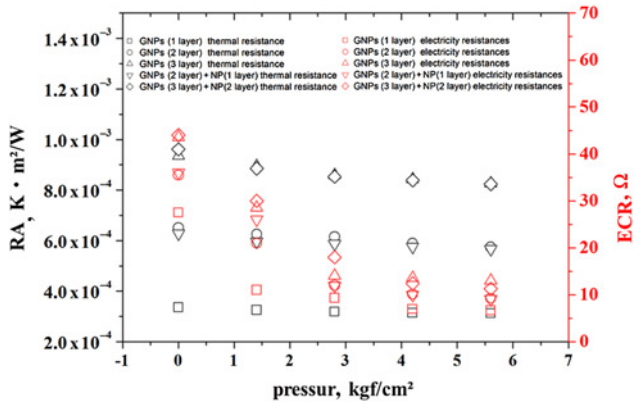

Figure 12 *Change in specific thermal resistance and electrical resistance with pressure for GNPs (one to three layers) and NPs (one and two layers) TIM during five tests, Q (34 W)*

5. Conclusion: The introduction of GNPs into TIMs has the potential for improving thermal conductivity. It is experimentally found that during compression and deformation, both thermal and electrical properties of the proposed hybrid conductive TIMs are highly correlated and the nature of thermal contact resistance variations with respect to electrical resistance can be deduced.

On the basis of the above results and discussion for the tested TIMs, the following conclusions can be drawn:

(i) The tested TIM composite samples of GNPs (one to three layers) and NPs (one and two layers) show a trend of decrease in specific thermal resistance values with increasing pressure. Decreased contact resistance between the interfaces with increasing pressure is found to be the main contributing factor.
(ii) The best thermal conductivity is obtained at ~0.2 W/m K at an applied pressure of 5.6 kgf/cm^2 for a thickness of 160 µm with three-layer GNPs and two-layer NPs TIM composite. Furthermore, the trend in the change of specific thermal conductivity with applied pressure is found to be consistent with the literature.
(iii) The experimental trend of slight increase in specific thermal resistance can be attributed to heat flux increase because of thickness increases in thermal expansion as the temperatures increase.
(iv) Electrical resistances at fabricated TIM composites of GNPs and NPs show a decreasing trend as the contact pressure is increased, similar to the trend of thermal resistance results.

6 References

[1] Prasher R.: 'Thermal interface materials: historical perspective, status, and future directions', *Proc. IEEE*, 2006, **94**, (8), pp. 1571–1586
[2] Chung D.D.L.: 'Thermal interface materials', *J. Mater. Perform.*, 2001, **10**, (1), pp. 56–59
[3] Boukhanouf R., Haddad A., North M.T., Buffone C.: 'Experimental investigation of a flat plate heat pipe performance using IR thermal imaging camera', *Appl. Therm. Eng.*, 2006, **26**, pp. 2148–2156
[4] Fletcher L.S.: 'A review of thermal enhancement techniques for electronic systems', *IEEE Trans. Compon. Hybrids Manuf. Technol.*, 1990, **13**, (4), pp. 1012–1021
[5] Hsieh W.H., Wu J.Y., Shih W.H., Chiu W.C.: 'Experimental investigation of heat-transfer characteristics of aluminum-foam heat sinks', *Int. J. Heat Mass Transf.*, 2004, **47**, pp. 5149–5157
[6] Skuriat R., Li J.F., Agyakwa P.A., Mattey N., Evans P., Johnson C.M.: 'Degradation of thermal interface materials for high-temperature power electronics applications', *Microelectron. Reliab.*, 2013, **53**, pp. 1933–1942
[7] Smith B., Brunschwiler T., Michel B.: 'Comparison of transient and static test methods for chip-to-sink thermal interface characterization', *Microelectron. J.*, 2008, **40**, (9), pp. 1379–1386
[8] Kempers R., Kolodner P., Lyons A., Robinson A.J.: 'A high-precision apparatus for the characterization of thermal interface materials', *Rev. Sci. Instrum.*, 2009, **80**, pp. 095111-1–095111-11
[9] Mahajan R., Chiu C.P., Chrysler G.: 'Cooling a microprocessor chip', *Proc. IEEE*, 2006, **94**, pp. 1476–1486
[10] Meysenc L., Jylhakallio M., Barbosa P.: 'Power electronics cooling effectiveness versus thermal inertia', *IEEE Trans. Power Electron.*, 2005, **20**, pp. 687–693
[11] Hui Y., Liangliang L., Yujun Z.: 'Silver nanoparticle-based thermal interface materials with ultra-low thermal resistance for power electronics applications', *Scr. Mater.*, 2012, **66**, pp. 931–934
[12] Schelling P.K., Shi L., Goodson K.E.: 'Managing heat for electronics', *Mater. Today*, 2005, **8**, pp. 30–35
[13] Lu D., Wong C.P., Prasher R., Chiu C.P.: 'Materials for advanced packaging' (Springer, New York, NY, 2009), pp. 437–458
[14] Xu Y.S., Chung D.D.L.: 'Increasing the thermal conductivity of boron nitride and aluminum nitride particle epoxy-matrix composites by particle surface treatments', *Compos. Interfaces*, 2000, **7**, pp. 243–256
[15] Prasher R.S., Shipley J., Prstic S., Koning P., Wang J.L.: 'Thermal resistance of particle laden polymeric thermal interface materials', *ASME J. Heat Transf.*, 2003, **125**, pp. 1170–1177
[16] Geim A.K., Novoselov K.S.: 'The rise of graphene', *Nat. Mater.*, 2007, **6**, pp. 183–191
[17] Chung D.D.L.: 'Exfoliation of graphite', *J. Mater. Sci.*, 1987, **22**, pp. 4190–4198

doi: 10.1049/mnl.2014.0689

[18] Dresselhaus M.S., Dresselhaus G., Eklund P.C., Chung D.D.L.: 'Lattice vibrations in graphite and intercalation compounds of graphite', *Mater. Sci. Eng.*, 1977, **31**, pp. 141–152
[19] Ganguli S., Roy A.K., Anderson D.P.: 'Improved thermal conductivity for chemically functionalized exfoliated graphite/epoxy composites', *Carbon*, 2008, **46**, pp. 806–817
[20] Sun X., Yu A., Ramesh P., Bekyarova E., Itkis M.E., Haddon R.C.: 'Oxidized graphite nanoplatelets as an improved filler for thermally conducting epoxy-matrix composites', *J. Electron. Packag.*, 2011, **133**, p. 020905
[21] Veca L.M., Meziani M.J., Wang W., *ET AL.*: 'Carbon nanosheets for polymeric nanocomposites with high thermal conductivity', *Adv. Mater.*, 2009, **21**, pp. 2088–2092
[22] Raza M.A., Westwood A., Brown A., Hondow N., Stirling C.: 'Characterisation of graphite nanoplatelets and the physical properties of graphite nanoplatelet/silicone composites for thermal interface applications', *Carbon*, 2011, **49**, pp. 4269–4279
[23] Veca L.M., Meziani M.J., Wang W., *ET AL.*: 'Carbon nanosheets for polymeric nanocomposites with high thermal conductivity', *Adv. Mater.*, 2009, **21**, pp. 2088–2092
[24] Xiang J.L., Drzal L.T.: 'Thermal conductivity of exfoliated graphite nanoplatelet paper', *Carbon*, 2011, **49**, pp. 773–778
[25] Xiaojuan T., Mikhail E.I., Elena B.B., Robert C.H.: 'Anisotropic thermal and electrical properties of thin thermal interface layers of graphite nanoplatelet-based composites'. Scientific Reports, 2013, vol. 10, p. 01710
[26] Xiang J.L., Drzal L.T.: 'Thermal conductivity of exfoliated graphite nanoplatelet paper', *Carbon*, 2011, **49**, pp. 773–778
[27] Song W.L., Ping W., Cao L., *ET AL.*: 'Polymer/boron nitride nanocomposite materials for superior thermal transport performance', *Angew. Chem., Int. Ed.*, 2012, **51**, pp. 6498–6501
[28] Fabris D., Rosshirt M., Cardenas C., Wilhite P., Toshishige Y., Cary Y.Y.: 'Application of carbon nanotubes to thermal interface materials', *J. Electron. Packag.*, 2011, **133**, p. 1115
[29] Nomura K.I., Ushijima H., Mitsui R., Takahashi S., Nakajima S.I.: 'Screen-offset printing for fine conductive patterns', *Microelectron. Eng.*, 2014, **123**, pp. 58–61
[30] Sekitani T., Someya T.: 'Ambient electronics', *Jpn. J. Appl. Phys.*, 2012, **51**, p. 100001
[31] Faddoul R., Bruas N.R., Blayo A.: 'Formulation and screen printing of water based conductive flake silver pastes onto green ceramic tapes for electronic applications', *Mater. Sci. Eng.*, 2012, **177**, pp. 1053–1066
[32] Yovanovich M.M.: 'Four decades of research on thermal contact, gap, and joint resistance in microelectronics', *IEEE Trans. Compon. Packag. Technol.*, 2005, **28**, (2), pp. 182–206
[33] Shenogina N., Shenogin S., Xue L., Keblinski P.: 'On the lack of thermal percolation in carbon nanotube composites', *Appl. Phys. Lett.*, 2005, **87**, p. 133106
[34] Itkis M.E., Borondics F., Yu A., Haddon R.C.: 'Thermal conductivity measurement of semitransparent single-walled carbon nanotube films by a bolometric technique', *Nano Lett.*, 2007, **7**, pp. 900–904